



Experimentally based water budgets for dehydrating slabs and consequences for arc magma generation

Max W. Schmidt^{a,*}, Stefano Poli^b

^a CNRS–UMR 6524, Magmas et Volcans, 5, rue Kessler, 63038 Clermont-Ferrand, France

^b Dip. Scienze della Terra, Sez. Mineralogia, Via Boticelli 23, 20133 Milano, Italy

Received 20 February 1997; revised version received 11 May 1998; accepted 4 June 1998

Abstract

Phase diagrams of hydrous mid-ocean ridge (MOR) basalts to 330 km depth and of hydrous peridotites to 250 km depth are compiled for conditions characteristic for subduction zones. A synthesis of our experimentally determined phase relations of chlorite, lawsonite, epidote-zoisite, amphibole, paragonite, chloritoid, talc, and phengite in basalts and of phase relations from the literature of serpentine, talc, chlorite, amphibole, and phase A in ultramafics permits calculation of H₂O contents in hydrous phase assemblages that occur in natural compositions. This yields the information necessary to calculate water budgets for descending slabs. Starting from low-grade blueschist conditions (10–20 km depth) with H₂O contents between 5 and 6 wt% for hydrated oceanic crust, complete dehydration is achieved between 70 and >300 km depth as a function of individual slab geotherms. Hydrous phases which decompose at depth below volcanic arcs are lawsonite, zoisite, chloritoid, and talc (\pm phengite) in mafic compositions and chlorite and serpentine in peridotite. Approximately 15–35% of the initially subducted H₂O are released below volcanic arcs. The contribution of amphibole dehydration to the water budget is small (5–20%) and occurs at relatively shallow depth (65–90 km). In any predicted thermal structure, dehydration is a combination of a stepwise and a continuous process through many different reactions which occur simultaneously in the different portions of the descending slab. Such a dehydration characteristic is incompatible with ‘single phase dehydration models’ which focus fluid flow through a unique major dehydration event in order to explain volcanic fronts. As a consequence of continuously progressing dehydration, water ascending from the slab will be generally available to depth of ca. 150–200 km. The fluid rising from the subducting lithosphere will cause partial melting in the hot portion of the mantle wedge. We propose that the volcanic front simply forms above the mantle wedge isotherm where the extent of melting is sufficient to allow for the mechanical extraction of parental arc magmas. Thermal models show that such an isotherm (ca. 1300°C) locates below volcanic fronts, slab surface depths below such an isotherm are compatible with the observed depths of the slab surface below volcanic fronts. © 1998 Elsevier Science B.V. All rights reserved.

Keywords: mid-ocean ridge basalts; magmas; island arcs; dehydration; slabs

* Corresponding author. Fax: +33 47334 6744; E-mail: max@opgc.univ-bpclermont.fr

1. Introduction

Volcanic arcs are the most spectacular testimony of destructive plate boundaries on the Earth's surface. Volcanic fronts, i.e. the onset of arc volcanism, form in correspondence to a depth of the subducting slab between 90 and 150 km, with a distribution maximum of 128 ± 38 km [1] or 110 ± 38 km (2σ) [2]. The width of volcanic arcs varies between 50 and 200 km.

It is widely accepted that arc volcanism is initiated through partial melting of a mantle wedge metasomatized by a fluid originating from dehydration of subducted crust [3–6]. The fundamental role of H₂O for island arc magmatism is also documented by an average H₂O content of 1.7 wt% in primitive island arc magmas contrasting mid-ocean ridge settings where primitive magmas have 0.1–0.5 wt% H₂O [7].

Recent efforts in determining the stability of hydrous phases at high pressures allow us to quantify the progressive dehydration of subducting slabs. The pressure–temperature stabilities of all major hydrous phases in the principal subducted lithologies (chlorite, lawsonite, epidote/zoisite, amphibole, chloritoid, talc, and phengite in gabbros, basalts, and sediments; serpentine, chlorite, amphibole, phase A, and talc in mantle compositions) are now experimentally determined. Mass balance calculations yield the relative contributions of individual hydrous phases to the transport of H₂O within the subducted lithosphere and between the subducted lithosphere and the overlying mantle wedge. The aim of this paper is to characterize and quantify the dehydration process. We present our experimental data on MOR basalt, discuss H₂O-saturated phase diagrams of basalt and peridotite, and compile *P*–*T* diagrams of calculated wt% (H₂O) bound in hydrous phases. On the basis of these data we draw implications and discuss models for the formation of the volcanic front.

2. Experimental procedure

Three different basaltic compositions (Table 1) were investigated, all of them being mixtures of synthetic glasses with Fe³⁺/Fe^{tot} ratios of 0.2–0.25 and synthetic and natural crystal seeds [8,9]. LTBC

Table 1
Bulk compositions

	LTBC	TB-1	KMB-7	MORB	hzb	lherz	pyrol
SiO ₂	52.05	51.58	50.59	52.4	44.5	45.3	45.1
TiO ₂	–	1.52	–	1.6	–	–	–
Al ₂ O ₃	16.75	16.68	18.96	16.9	1.7	3.6	3.5
Cr ₂ O ₃	–	–	–	–	–	–	0.4
Fe ₂ O ₃	2.26	1.83	1.81	–	–	–	0.5
FeO	7.41	8.31	8.24	10.3 ^a	9.6 ^a	7.3 ^a	8.0
MgO	7.30	7.02	6.93	7.1	42.6	40.3	37.5
CaO	10.01	9.90	10.08	10.1	1.4	3.0	3.1
Na ₂ O	3.18	3.16	2.90	3.2	0.1	0.3	0.6
K ₂ O	–	–	0.49	0.1	–	–	0.1

The first three compositions are basaltic starting materials, the others averages for MOR basalt, harzburgite (hzb), lherzolite (lherz) [57] and pyrolite (pyrol) [58].

^aTotal iron as FeO.

is close to a Na₂O–CaO–FeO–MgO–Al₂O₃–SiO₂–H₂O system, KMB contains additional K₂O, TB additional TiO₂. Experiments contained 5 wt% H₂O at pressures to 40 kbar and 2 or 1 wt% H₂O at higher pressures. All experiments were fluid-saturated and in piston cylinder experiments oxygen fugacity was buffered to NNO conditions by a double capsule technique.

A total of 63 experiments were performed at pressures between 18 and 120 kbar and temperatures between 550 and 1100°C. Run times varied from 629 h (18 GPa, 550°C) to 30 h (above 800°C, 50 kbar; run table in **EPSL Online Background Dataset**¹). Experiments to 36 kbar were performed in an end-loaded piston cylinder apparatus with a half-inch bore. Full salt assemblies with a tapered graphite heater were employed [8,10]. Experiments above 40 kbar were performed in a split sphere multi-anvil apparatus (MA-8) at the Bayerisches Geoinstitut. An 18-mm edge length octahedra (18M) with a stepped graphite furnace was employed on an 11-mm truncation edge length (TEL) for experiments to 100 kbar and a 14M octahedra with a stepped LaCrO₃ furnace was employed on an 8-mm TEL for experiments above 100 kbar (for details see [11]). Thermocouples were of Pt–Pt₉₀Rh₁₀ and situated in direct contact to the capsules of 1.5–2.0 mm ini-

¹ <http://www.elsevier.nl/locate/epsl>, mirror site:
<http://www.elsevier.com/locate/epsl>

tial length. Calibrations were against quartz–coesite, fayalite–spinel, and coesite–stishovite for the 18M assemblage [11] and against coesite–stishovite and Mg_2SiO_4 forsterite- β -phase at 1200°C for the 14M assemblage.

3. MOR basalt

3.1. Experimental results

Experiments between 18 and 120 kbar and 550 and 1100°C of this study and experiments of previous

work [8,10] are compiled in Fig. 1. All experiments of this study contain garnet and omphacite, thus represent eclogitic assemblages. Several hydrous phases occur at pressures above the amphibole stability: lawsonite, zoisite, chloritoid, and occasionally talc or staurolite. In potassium-bearing basalt phengite appears ubiquitous at subsolidus conditions.

Most experiments represented in Fig. 1 were conducted with two or three different basaltic compositions (TB, KMB, and LTBC). Resulting phase assemblages for the three bulk compositions were identical with the following exceptions. The potassium-bearing basalt KMB has an additional potas-

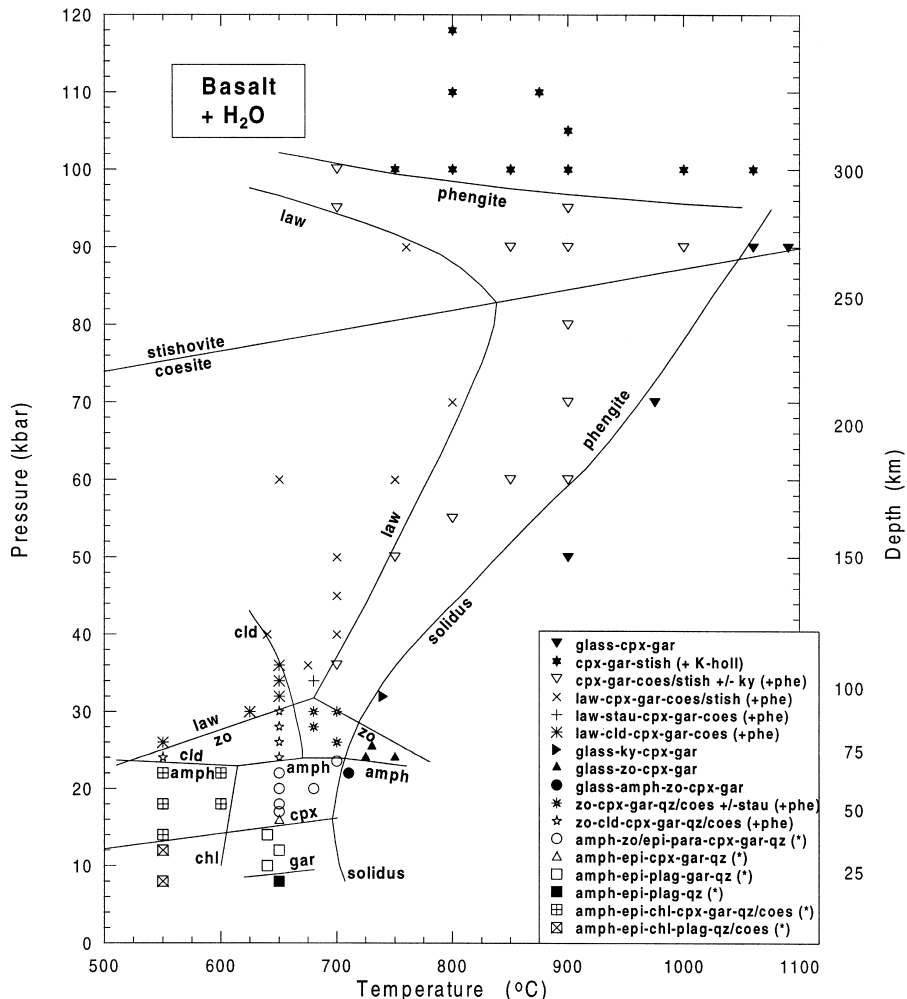


Fig. 1. Experimentally determined phase relationships for water-saturated MOR basalt: *amph* = amphibole, *chl* = chlorite, *cld* = chloritoid, *cpx* = jadeitic or omphacitic clinopyroxene, *epi* = epidote, *gar* = garnet, *law* = lawsonite, *zo* = zoisite.

sium phase (phengite or K-hollandite) at subsolidus conditions. The high temperature stability of chloritoid differs for about 20–40°C for the different basalts. The appearance of some minor phases differs slightly between the different basalts: in LTBC talc appears in a few experiments (32–26 kbar at 650°C); staurolite occurs in some experiments (preferentially in TB) between 25 and 30 kbar, 650–700°C; and at conditions above 30 kbar, 700°C minor kyanite occurs in some experiments (LTBC and KMB).

Clinopyroxene forms a matrix of small (3–15 µm) euhedral crystals. Jadeite and diopside seeds disappeared completely and clinopyroxenes were in each experiment. Jadeite fractions are mostly between 0.40 and 0.50 but increase to 0.60–0.65 above 90 kbar when garnets become majoritic (Table 2). At about 40 kbar, K₂O contents in clinopyroxene (in KMB) become significant and increase systematically with pressure to a maximum of

1.2 wt% at 100 kbar (Fig. 2). K₂O contents of clinopyroxene increase with temperature until the solidus is reached but at supersolidus conditions the KAlSi₂O₆-component decreases drastically.

Garnets form texturally equilibrated crystals but often preserve cores which are intermediate between seed and rim compositions. In most experiments rims around grossular-, pyrope- or almandine-rich cores are identical in composition, but in some runs of shorter duration equilibration of rims was incomplete. Between 25 and 90 kbar the pyrope component in garnet increases slightly. At about 90 kbar garnets become majoritic and silica contents increase to ca. 3.15 Si per formula unit (pfu) at 110 kbar. Simultaneously, the grossular component decreases by about 15 mol% (e.g. in KMB from gros₃₅ to gros₂₀).

Lawsonite crystallizes anew and forms rectangular-shaped euhedral crystals of 7–20 µm in size. Lawsonite compositions are close to endmember compositions, impurities are 0.3–0.8 wt% FeO, 0.2–

Table 2
Average phase compositions

	Clinopyroxene			Garnet			Law	Zoisite	Cld	Stau	Phengite	
P (kbar):	26	90	111	70	100	110	90	30	32	26	80	90
T (°C):	700	850	870	900	900	800	750	700	650	700	900	850
Bulk:	TB	KMB	TB	KMB	KMB	TB	KMB	TB	TB	TB	KMB	KMB
SiO ₂	56.10	54.84	57.50	40.93	41.29	41.76	38.42	39.17	26.37	29.45	57.45	59.57
TiO ₂	0.02	—	0.37	—	—	1.52	—	0.20	0.02	0.41	—	—
Al ₂ O ₃	12.51	10.57	15.02	22.87	20.11	21.06	30.12	31.52	41.51	56.78	16.67	11.89
Fe ₂ O ₃	0.00	0.36	0.45	0.00	0.49	0.00	0.14	2.37	1.64	0.00	0.00	0.00
FeO	4.65	7.25	2.72	14.20	19.94	15.14	0.63	0.00	14.50	6.51	1.68	3.40
MgO	8.16	8.58	6.41	10.12	10.17	7.50	0.45	0.04	8.21	5.83	7.10	8.72
CaO	12.73	11.79	8.78	12.19	7.08	13.28	16.87	24.32	0.48	0.29	0.08	0.09
Na ₂ O	6.76	6.19	9.01	0.17	0.35	0.69	0.18	0.00	0.35	0.00	0.08	0.08
K ₂ O	—	0.57	—	0.05	0.20	—	0.02	—	—	—	10.84	10.81
H ₂ O	—	—	—	—	—	—	11.28	1.96	7.65	1.11	4.45	4.45
Total	100.94	100.15	100.26	100.53	99.63	100.95	98.51	99.57	100.73	100.40	98.36	99.00
Si	1.973	1.975	1.999	3.024	3.125	3.118	2.064	3.001	2.065	7.949	3.867	4.018
Ti	0.001	—	0.010	—	—	0.085	—	0.012	0.001	0.083	—	—
Al	0.519	0.449	0.615	1.991	1.794	1.854	1.887	2.846	3.831	18.063	1.322	0.945
Fe ³⁺	0.000	0.010	0.012	0.000	0.028	0.000	0.005	0.137	0.097	0.000	0.000	0.000
Fe ²⁺	0.137	0.218	0.079	0.877	1.262	0.946	0.028	0.000	0.949	1.470	0.095	0.192
Mg	0.428	0.461	0.332	1.114	1.147	0.835	0.036	0.004	0.958	2.346	0.713	0.877
Ca	0.480	0.455	0.327	0.965	0.574	1.063	0.961	1.996	0.040	0.084	0.006	0.007
Na	0.461	0.432	0.607	0.024	0.052	0.100	0.018	0.000	0.054	0.000	0.010	0.010
K	—	0.026	—	0.005	0.019	—	0.002	—	—	—	0.931	0.930
H	—	—	—	—	—	—	4.000	1.000	4.000	2.000	2.000	2.000

Fe³⁺ calculated from charge balance for lawsonite, chloritoid, and staurolite. Staurolite normalized for 15 cations and 24 oxygens including 1(OH) group. Mica formulas on 11 oxygens and 2(OH), all Fe²⁺. Abbreviations as in Fig. 1.

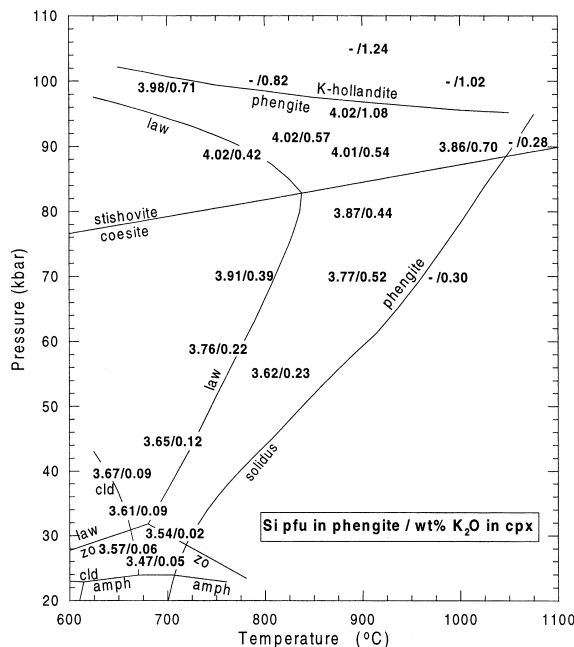


Fig. 2. Compositions of phengite (in Si per formula unit, given only in the phengite stability field) and clinopyroxene (in wt% K₂O) in MOR basalt.

0.5 wt% MgO, and maximal 0.6 wt% TiO₂. Zoisite is present in all runs below 32 kbar which do not contain lawsonite. Zoisite forms large (15–30 μm) crystals which rarely preserve almost Fe-free cores (present in the starting material). Equilibrium compositions are constant at 0.14–0.18 Fe pfu (Table 2).

Phengite is present in all subsolidus experiments (bulk composition KMB) to 95 kbar. In most experiments, phengite tablets are larger than 15 μm which allows measurement with defocused beam. Generally, the celadonite component increases with pressure and decreases slightly with temperature (Fig. 2). Around 90–95 kbar, phengite reaches an endmember celadonite composition and decomposes with further increase of pressure. In experiments above 50 kbar with 2–3 wt% of free fluid phase, an enrichment of potassium along grain boundaries could be detected in backscatter images. However, the resolution of the microprobe did not permit to identify the origin of this enrichment. K-hollandite which replaces phengite towards higher pressure was extremely rare in the experimental charges. In most experiments only a few rectangular-shaped grains of 5 to 20 μm with

almost ideal compositions (KAlSi₃O₈) have been found.

Chloritoid appears as aggregates of 10–40 μm in size. An increase of magnesium number with temperature is observed. At pressures between 26 and 30 kbar and at temperatures above the chloritoid stability (see Fig. 1), staurolite occurs occasionally (mostly bulk composition TB). Staurolites form small euhedral crystals of 5–10 μm size. Talc occurs in some experiments with LTBC composition. It forms relatively large crystals of 10–20 μm.

Interstitial liquid forms in small amounts (<5–10%) above the solidus; compositions could not be measured. When liquid forms, phengite and quartz/coesite/stishovite disappear. In the scanning electron microscope it appears that quenched liquids contain frequently small (<2 μm) euhedral garnets and sometimes liquid is partly replaced by quench crystals of submicron size.

3.2. Petrological evolution of subducting basalt

Phase relationships of MOR basalt at water-saturated conditions are compiled in Figs. 1 and 3. For the low-temperature region ($\leq 550^{\circ}\text{C}$) assemblages from natural blueschists are employed. The subsolidus region below 8 kbar was experimentally investigated by Apted and Liou [12] and from 8 to 24 kbar by Poli [8]. The experiments by Pawley and Holloway [13] at pressures from 20 to 30 kbar are consistent with our experiments.

During subduction, the oceanic crust passes through a blueschist facies stage (10–50 km depth). Natural blueschists of basaltic origin are mostly fully hydrated while coarse-grained gabbros [14] often show domainal equilibria resulting from uneven water distribution. A general sequence of hydrous phases in basalt with increasing pressure might be described as follows. At blueschist conditions, assemblages are typically composed of lawsonite–glaucophane–chlorite–albite/jadeite ± phengite (fields G and K, Fig. 3). With increasing temperature lawsonite reacts to epidote/zoisite (fields F, I, and J), chlorite decomposes forming mainly garnet (fields E and H), and glaucophane changes composition to barrosoitic amphibole. At temperatures above 600°C, pressures from 15 to 22 kbar, an amphibole–eclogite results (field E). When

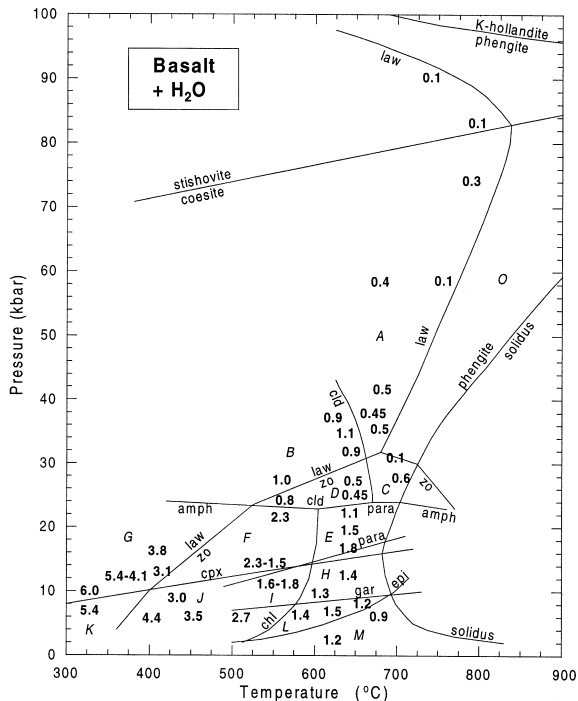
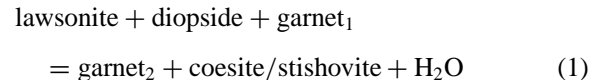


Fig. 3. Maximum H₂O contents bound in hydrous phases in H₂O-saturated MOR basalt. For assemblages and references see Table 3.

pressure oversteps 22–24 kbar, amphiboles decompose forming chloritoid at temperatures below 660°C (fields B and D). Blueschists transform to lawsonite-eclogites (fields A and B) and amphibole-eclogites to zoisite-eclogite (fields C and D). At ca. 30 kbar zoisite reaches its maximum stability in metabasalts (at $f_{\text{O}_2} = \text{NNO}$), its breakdown leaves an almost dry eclogite at conditions above 30 kbar, 700°C (field O). At lower temperatures, lawsonite persists reaching its maximum temperature stability at 830°C, 84 kbar (field A). If potassium is present in a subducted MOR basalt, phengite forms ubiquitously to pressures of 100 kbar [9]. The presence of phengite also determines minimum melting conditions of MOR basalts at high pressures.

Other minor hydrous phases in MOR basalt are paragonite, talc, and staurolite. Paragonite forms at 12–16 kbar (at 500–650°C) and decomposes around 22 kbar (500–700°C, field E and part of field F). The conditions of talc and staurolite occurrence are relatively restricted, although talc is probably an important high-pressure phase in Mg-gabbros.

Most of the reactions involved are discussed by [8,10]. We complete the discussion of phase relations with the lawsonite and phengite breakdown reactions at high pressures. At pressures above the zoisite stability, lawsonite decomposes through a continuous reaction of the type



where garnet₂ is richer in grossular and pyrope component than garnet₁. In the coesite stability field, this reaction has a positive ΔV and a positive dP/dT slope which steepens with increasing pressure (Fig. 1). When stishovite replaces coesite, ΔV of reaction becomes negative. Thus, above 80 kbar, reaction (1) has a negative dP/dT slope and thus limits the maximum pressure stability of lawsonite in subduction zones to 80–90 kbar.

White mica, the principal potassium host in natural blueschists and eclogites, decomposes through a continuous and a discontinuous reaction. At pressures above 40 kbar, a significant solubility of potassium in clinopyroxene is observed and phengite decomposes forming KAlSi_2O_6 -cpx + enstatite + coesite + K-rich fluid [9]. This reaction is continuously progressing from 40 kbar until the terminal phengite stability near 100 kbar is reached. The discontinuous breakdown of phengite to K-hollandite (KAlSi_3O_8) + clinopyroxene + K-rich fluid and the related dehydration might be of small significance in basaltic compositions. Mass balance calculations on the basis of the experiments reveal that in MOR basalts (0.1–0.5 wt% K_2O) phengite may react completely to K-cpx before the pressure stability of phengite is reached (Fig. 4). With a potassium solubility in clinopyroxene of about 1 wt% (at 100 kbar) and a modal amount of 40–50 wt% cpx, 0.4–0.5 wt% bulk- K_2O can be stored in clinopyroxene.

3.3. Mass balance

Modal amounts of phases in basalt (Table 3) are compiled from natural blueschists with basaltic chemistry [15–19], from [12] and from our own experiments. For a description of modal amount calculations in basalt see [8]. Fig. 3 gives wt% of H₂O in the bulk rock bound in hydrous phases. These

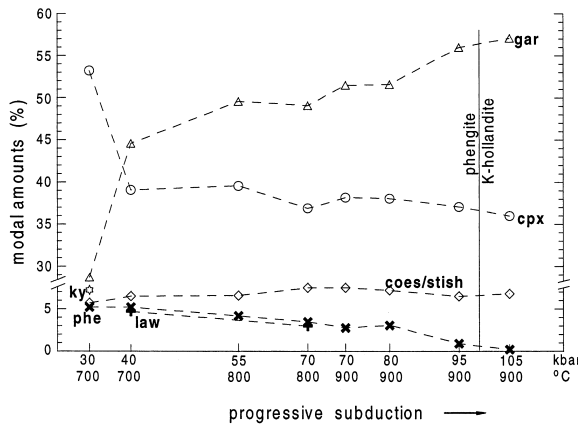


Fig. 4. Modal amounts of phases in MOR basalt with 0.5 wt% K₂O along a typical subduction geotherm. Phengite continuously decomposes when potassium solubility in clinopyroxene increases.

values are for potassium-free basalt. For potassium-bearing basalt 0.5 wt% H₂O (equivalent to 8–9 wt% phengite) must be added per 1 wt% K₂O. Our results are comparable to those of [20] which estimated water contents for subducting oceanic crust to 40 km depth.

As can be seen from Fig. 3, many different reactions involving hydrous phases modify the water contents during the transition from blueschists to dry eclogites. Water contents will continuously decrease because most of the reactions are continuous reactions involving solid solutions and thus take place over a

temperature/pressure interval [21]. In an experimental study [8] it was shown that continuous amphibole decomposition in amphibole eclogite (field H and E in Fig. 3) causes as much dehydration as the final amphibole breakdown (each ΔH₂O^{tot} = 0.6 wt%).

The phases with large contributions to the water budget of subducting MOR basalt are lawsonite, chlorite, and amphibole (glaucophane or barroisite in composition). Lawsonite contains 11.2 wt% H₂O and typically amounts to 7–15 wt%. Chlorite in basalt contains about 12 wt% H₂O and amounts to 5–30 wt%. Amphibole only contains 2.1 wt% H₂O but forms 20–60 wt% of a basalt. Other significant contributions arise from epidote/zoisite (1.95 wt% H₂O) which forms typically 5–20 wt%, and from chloritoid (7.5 wt% H₂O) amounting to 3–8 wt%. Paragonite (4.6 wt% H₂O), talc (4.8 wt% H₂O), and staurolite (1.0 wt% H₂O) have only minor contributions due to medium–low water contents in combination with relatively low modal abundances.

The following dehydration characteristics can be defined. In the shallow portion of the subducting slab, basalts typically contain 5–6 wt% H₂O. With increasing pressure (but still in the stability field of amphibole), water contents decrease to ca. 3 wt% at low temperatures where lawsonite + chlorite + glaucophane is stable, to 2.0–2.5 wt% at intermediate temperatures where epidote + chlorite + glaucophane/barroisite is stable, and to 1–1.5 wt% where epidote/zoisite + barroisite is stable.

Table 3
Assemblages, modal amounts of hydrous phases (wt%) and H₂O (wt%) bound in hydrous phases in MOR basalt

Field in Fig. 3	Assemblage	Ranges for modal amounts of hydrous phases	Range of H ₂ O ^{tot}	References
O	gar–cpx–coes/stish	—	0.0	
A	law–gar–cpx–coes/stish	1–5 law	0.1–0.5	[10], this study
B	law–cld–gar–cpx–qz/coes	4–7 law, 4–10 cld	0.9–1.1	[10], this study
C	zo–gar–cpx–qz/coes	1–4 zo; (13 zo, 8 tc)	0.1–0.6	this study, ([19])
D	zo–cld–gar–cpx–qz/coes	3–5 zo, 5–9 cld	0.5–0.8	[8], this study
E	amph–zo–epi–para–gar–cpx–qz	22–60 amph, 16–20 epi, 4–6 para	1.1–1.8	[8]
F	amph–zo–chl± para–gar–cpx–qz	22–48 amph, 9–22 epi, 4–12 chl, 0–5 para	1.5–2.3	[8,17]
G	law–chl–glauc–gar–cpx–qz	35–45 amph, 22–36 law, 0–13 chl	3.1–6.0	[10] ^a ,[15]
H	amph–epi–plag–gar–qz	45–58 amph, 9–14 epi	1.2–1.4	[8,16]
I	amph–epi–chl–plag–gar–qz	25–26 amph, 7–11 epi, 8–9 chl	1.6–1.8	[17]
J	amph–epi–chl–ab/plag–qz	12–35 amph, 15–30 chl, 25–34 epi	2.7–4.4	[12,18]
K	law–amph–chl–ab–qz	58 amph, 34 law, 4 chl	5.4	[10] ^a
L	epi–amph–plag–qz	39–62 amph, 8–30 epi	1.2–1.5	[8,12,16]
M	amph–plag–qz	45–60 amph	0.9–1.2	[12]

^a [10]: references in Ref. [10], Ref. [19] is from a coesite bearing gabbro.

The most significant discontinuous reactions in the amphibole stability field are the formation of omphacitic clinopyroxene and the breakdown of chlorite. At pressures exceeding the stability of amphibole (>22–24 kbar), ca. 1 wt% H₂O remain bound in lawsonite and chloritoid (<520°C) and 0.5–0.7 wt% H₂O bound in zoisite ± chloritoid. At higher pressures (>30–40 kbar) when lawsonite constitutes the only non-potassic hydrous phase, the bulk water content is typically 0.2–0.5 wt% H₂O.

Apart from the continuity of several reactions, temperature gradients and compositional variations in the descending oceanic crust will further broaden the dehydration signal. Temperature gradients within a 7–10 km thick oceanic crust are 100–300°C [22]. Consequently, several dehydration reactions may take place at the same depth. Strictly, these calculations and phase relationships are only valid for MOR basaltic compositions. However, the stabilities of lawsonite, epidote/zoisite, amphibole, and chlorite are relatively insensitive to bulk rock composition [10]. On the contrary, ferromagnesian phases such as chloritoid and talc will have significantly enlarged stability fields and abundances in Mg-gabbros as can be deduced from field occurrences ([23] and references therein).

4. Metapelites and metagreywackes

Metapelites and metagreywackes constitute on average the upper 10% of the oceanic crust. Although they contribute only a small portion to the water budget, they are important for hosting the vast amount of certain elements or isotopes characteristic for the sediment-signature in arc magmas (K, Rb, Ba, Sr, ¹⁰Be, enrichment in ²⁰⁷Pb [3,5,6]). Phase relations for sedimentary materials metamorphosed at subduction zone conditions were experimentally studied by [24–26].

Chlorite + kyanite and staurolite + quartz are limited to pressures below 20 kbar for most natural bulk compositions, the latter having Mg/(Mg + Fe) ratios of 0.3–0.6. At pressures above 20 kbar, hydrous assemblages comprise talc–chloritoid–phengite or talc–phlogopite–phengite. Between 40 and 50 kbar talc + kyanite destabilizes and Mg-Al–pumpellyite (7.1 wt%

H₂O) and/or topaz–OH (10.7 wt% H₂O) might form in the presence of phengite. Metagreywackes are commonly richer in Ca than metapelites and thus lawsonite or zoisite are more abundant. The stability field of lawsonite in metapelite [26] is very similar to that in mafic systems. H₂O storage in sediments to more than 200 km depth is ensured by phengite, lawsonite, MgAl–pumpellyite, and topaz–OH at temperatures as high as 900°C.

5. Peridotites

The principal hydrous phases in H₂O-saturated peridotite to 80 kbar are serpentine, phase A, chlorite, talc, and amphibole. Stabilities of serpentine, phase A, and talc are expected to be almost identical for depleted or fertile peridotite because these phases are almost Ca- and Na-free and contain only minor amounts of Al₂O₃. Their stabilities have been experimentally determined on natural mineral compositions [27,28]. The stabilities of chlorite and amphibole are expected to vary for harzburgitic, lherzolitic, and pyroilitic bulk compositions. Mysen and Boettcher [29] determined a stability increase of amphibole from ca. 22 kbar in harzburgite to ca. 25 kbar in enriched lherzolite (at 800–1000°C).

Serpentine contains 12.3 wt% H₂O and dominates, together with chlorite (13.0 wt% H₂O), the water budget of hydrous peridotite to ca. 150 km depth. In natural peridotites serpentine forms during low-grade hydration, and its maximum temperature stability is 720°C (21 kbar, invariant point 3 in Fig. 5). Serpentine (antigorite, Mg₄₈Si₃₄O₈₅(OH)₆₂) decomposes to talc + olivine + H₂O below 21 kbar [27], to orthopyroxene+olivine + H₂O from 21 to 62 kbar, and to phase A + orthopyroxene + H₂O [28] at higher pressures (invariant point 4 in Fig. 5).

In average mantle compositions, *talc* (4.7 wt% H₂O) + olivine have a rather limited stability field less than 100°C wide, and they decompose to enstatite + H₂O between 690°C (10 kbar) and 720°C (20 kbar) [28]. In relatively silica-rich veins, talc might locally persist to higher temperatures and pressures [30,31].

In subducted peridotite, *phase A* (Mg₇Si₂O₈(OH)₆, 11.8 wt% H₂O) replaces serpentine at pressures between 60 and 70 kbar through

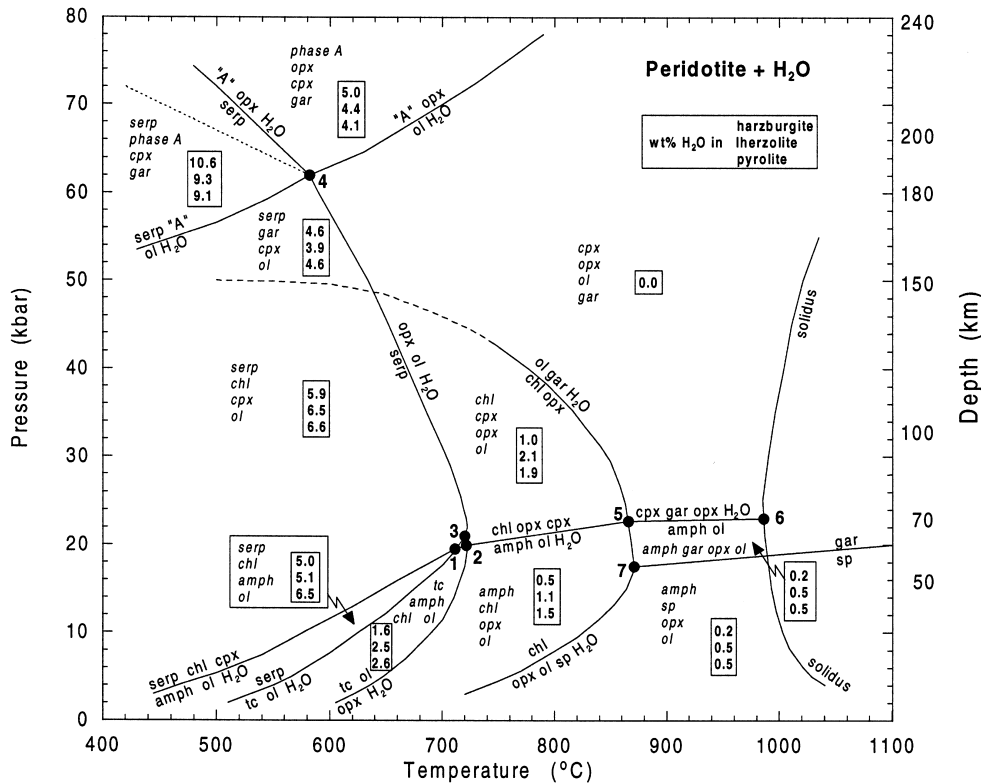


Fig. 5. Phase diagram for H₂O-saturated average mantle peridotite and maximum H₂O contents bound in hydrous phases in average peridotites. Upper value: harzburgite; middle value: lherzolite; lower value: pyrolite. The italic labels are assemblages in a given stability field. 'A' = phase A, *amph* = amphibole, *chl* = chlorite, *cpx* = clinopyroxene, *gar* = garnet, *ol* = olivine, *opx* = orthopyroxene, *serp* = serpentine, *sp* = spinel, *tc* = talc.

a water-conserving reaction (dotted line emerging from invariant point 4 in Fig. 5). Although phase A could form at lower pressures through olivine + H₂O = phase A + serpentine, the free water necessary for this reaction would not be available in subducting peridotite. Above 62 kbar, phase A + orthopyroxene decompose with increasing temperature to enstatite + H₂O. This reaction has a moderate positive slope in *P-T* space [32].

In natural peridotites, chlorites have compositions close to clinochlor ($Mg_5Al_2Si_3O_{10}(OH)_8$). Synthetic clinochlor decomposes between 3 and 21 kbar to olivine + orthopyroxene + spinel + H₂O with a maximum temperature stability of 870°C ([31] and references therein). Above 21 kbar, the occurrence of chlorite in peridotite is limited through the reaction chlorite + orthopyroxene = olivine + garnet + H₂O. This reaction was experimentally determined to pressures of 40 kbar [33]. Although considerable

uncertainty remains, it can be deduced from experiments on the terminal stability of chlorite [34] that the stability of chlorite + orthopyroxene do not exceed 50 kbar. The stability of chlorite outlined in Fig. 5 represents probably a maximum, and Fe could decrease the stability of chlorite in natural peridotite significantly.

5.1. Amphibole in peridotite

A compilation of all experimental studies on amphibole in water-saturated peridotite compositions yields the following picture. Close to the water-saturated solidus (approximately 1000°C, at 20–30 kbar), amphibole is pargasitic hornblende in composition and decomposes between 22 and 30 kbar. In harzburgite, calcic amphibole decomposes at 22 kbar, in lherzolite at 25–28 kbar and in enriched pyrolite at 28–30 kbar [29,35–37]. Mysen and Boettcher

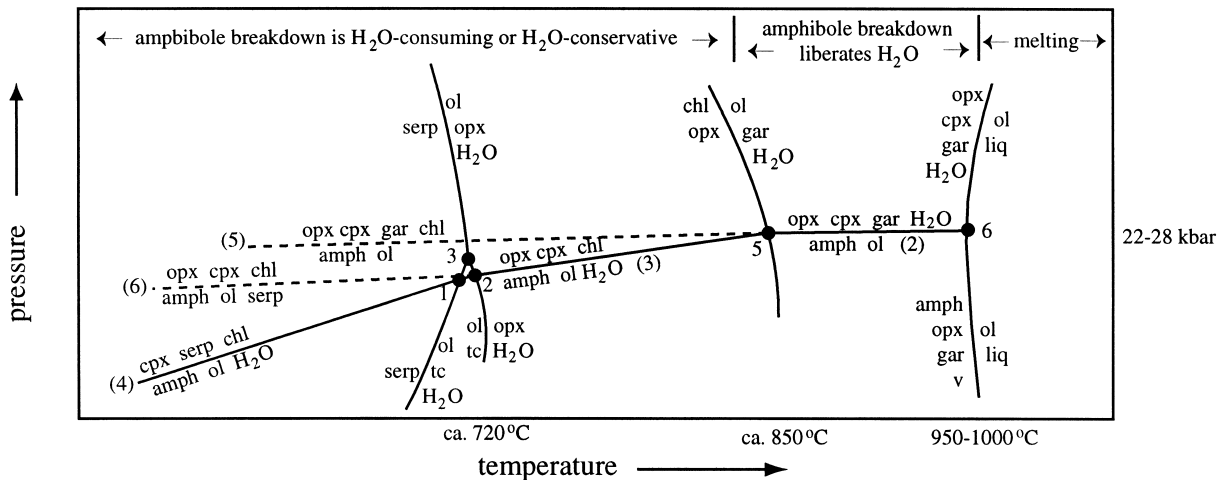


Fig. 6. Result of Schreinemakers analysis for breakdown reactions of amphibole in peridotite. The solid lines are amphibole breakdown reactions in a system where excess water is present, the stippled lines represent amphibole breakdown reactions in a fluid-absent system. The highest pressure where amphibole is stable is located at the solidus. Numbers without parentheses refer to invariant points in Fig. 5. The amphibole breakdown reaction between invariant point 1 and 2 is $\text{amph} + \text{ol} + \text{H}_2\text{O} = \text{tc} + \text{cpx} + \text{chl}$. Abbreviations as in Fig. 5.

[29] determined experimentally a slightly positive P - T slope for the amphibole-out reaction at subsolidus conditions. Calculations of the P - T slope of the amphibole-out reaction (2) of Fig. 6 agree with [29] yielding 3 to -1 bar/K as a function of exact amphibole-composition and solid solution model (molar volumes and entropies from 1996 update of [38]). Consequently, the highest pressure stability of amphibole is located at the intersection of the amphibole-out curve with the solidus, i.e. between 22 and 30 kbar (65–90 km depth). With decreasing temperature, this pressure is reduced by several kbar (Figs. 5 and 6). The experimental evidence is in sharp contrast to Tatsumi [2] who extrapolates the slope of Millholen et al.'s [35] amphibole melting curve into the subsolidus in order to reach 35 kbar at 700°C. The amphibole-out reaction near the solidus does not shift as a function of the bulk H_2O content: as long as the volatile species is only water, reaction (2) of Fig. 6 does not change position in P - T space. When the fluid is diluted by components other than H_2O , this reaction is shifted to lower pressures, consequently, H_2O -saturated bulk compositions yield the highest amphibole stabilities.

At temperatures where chlorite appears instead of garnet, reaction (2) transforms into reaction (3) (Fig. 6). Calculated P - T slopes for the latter reaction are positive and range from 11 to 13 bar/K. The

amphibole breakdown reactions (3) and (4), latter in the chlorite + serpentine stability field, do not liberate water. On the contrary, in a water-saturated system, the decomposition of amphibole consumes water with increasing pressure. In the descending slab, additional water is not necessarily available and amphibole decomposes through water conserving reactions (5) and (6) (Fig. 6). Thus, it is only at temperatures above the chlorite stability that the amphibole breakdown liberates water.

The exact stoichiometries of the amphibole decomposition reactions are complicated by the change of amphibole composition with temperature. From experiments and natural xenoliths it is known that at temperatures near the solidus amphibole is pargasitic hornblende in composition. In low temperature–high pressure metamorphic peridotites, amphiboles are aluminous tremolites. For the pressure breakdown reactions we thus continuously interpolated between these two amphibole compositions. Fig. 6 is valid for amphibole compositions to be expected in natural peridotite; however, reaction topologies are different for endmembers such as tremolite or edenite.

5.2. Water contents in fully hydrated peridotite

Modal abundances in hydrous peridotite assemblages are calculated employing a least-square

Table 4

Modal amounts (wt%) and maximum H₂O contents (wt%) bound in hydrous phases in hydrous peridotites

Assemblage	Herzolite solid phases			Lherzolite H ₂ O ^{tot}	Pyrolite H ₂ O ^{tot}	Harzburgite solid phases		Harzburgite H ₂ O ^{tot}			
serp-chl-cpx-ol	37.9	15.7	13.4	33.0	6.5	6.6	41.0	7.8	6.1	45.1	5.9
serp-gar-cpx-ol	32.3	11.9	10.6	45.3	3.9	4.3	38.4	5.9	4.6	51.2	4.6
serp-gar-cpx-phase A	59.2	11.2	10.0	19.6	9.3	9.1	68.2	5.5	4.3	22.1	10.6
phase A-gar-cpx-opx	38.4	11.8	10.5	39.2	4.4	4.1	44.1	5.8	4.6	45.5	5.0
serp-chl-amph-ol	25.8	12.2	21.2	40.7	5.1	6.4	33.9	6.2	9.9	50.0	5.0
talc-chl-amph-ol	8.9	12.5	21.8	56.8	2.5	2.6	11.7	6.4	10.3	71.7	1.6
opx-chl-amph-ol	14.7	5.1	22.1	58.1	1.1	1.5	17.2	2.5	10.4	69.9	0.5
opx-chl-cpx-ol	17.4	16.4	14.0	51.9	2.1	1.9	19.1	8.2	6.4	66.3	1.0
opx-sp-amph-ol	16.7	0.2	22.2	61.0	0.5	0.5	18.1	0.1	10.4	71.4	0.2
opx-gar-amph-ol	16.0	1.7	21.3	60.9	0.5	0.5	17.7	1.1	9.9	71.4	0.2
opx-gar-cpx-ol	15.7	13.0	10.3	61.0	0.0	0.5	18.1	6.4	4.6	71.0	0.0

fit procedure. FeO + MgO, Al₂O₃ + Fe₂O₃ + Cr₂O₃, and Na₂O + K₂O were each reduced to a single chemical component. Serpentine and chlorite compositions were held constant at the ideal stoichiometries of antigorite and clinochl. This introduces a small error for the calculated abundances of chlorite. By varying the alumina content of clinochl for ±20%, relative differences in the calculated H₂O^{tot} contents are -11/+16% for the assemblage chlorite–amphibole–orthopyroxene–olivine and -17/+26% for chlorite–clinopyroxene–orthopyroxene–olivine. Amphibole compositions were varied with temperature as described above. The relative amounts of clinopyroxene and amphibole depend on their Na:Ca ratios. Since compositional data at low temperatures are scarce, we allowed amphibole to completely replace clinopyroxene. This results in maximum amphibole and minimum chlorite abundances.

The results of the mass balance calculations for average peridotite compositions (Table 1) are presented in Table 4 and Fig. 5. In the stability fields of serpentine and phase A the total amount of H₂O bound in hydrous phases varies between 3.9 and 10.6 wt% of the bulk rock. In the stability field of serpentine + chlorite + amphibole, chlorite contributes approximately 30% (lherzolite) of the H₂O bound in hydrous phases, whereas amphibole contributes less than 10% (Table 4). When serpentine reacts to talc, H₂O contents decrease from 5.1 to 2.5 wt% in lherzolite. At higher temperatures, when chlorite + amphibole constitute the stable hydrous phases,

H₂O contents decrease to 1.1 wt% in lherzolite (0.5 wt% in harzburgite). In this assemblage chlorite contributes about 60% whereas amphibole contains 40% of the H₂O bound in hydrous phases. When chlorite is the only hydrous phase, H₂O contents are 2.1 wt% in lherzolite (1.0 wt% in harzburgite). When amphibole is the only stable hydrous phase, H₂O contents amount to less than 0.5 wt% in lherzolite (0.2 wt% in harzburgite). In chlorite/amphibole assemblages, water contents are higher in fertile than in depleted peridotite, because higher Na₂O, CaO, and Al₂O₃ contents result in larger amounts of amphibole and chlorite.

Serpentine has a predominant role in the water budget of peridotite. When serpentine decomposes, chlorite becomes the dominant hydrous phase. Although amphibole contains ca. 40% of the H₂O bound in the *P-T* domain of chlorite + amphibole, water is not liberated when amphibole decomposes. It is only between 800–850°C and the wet solidus (ca. 1000°C) that fluids result from the breakdown of amphibole. The quantity of this fluid is small compared to the fluid resulting from other phases: in lherzolite, the maximum content of amphibole amounts to 19 wt% (harzburgite 9 wt%) contributing a maximum of 0.5 wt% (harzburgite 0.2 wt%) H₂O. Recently, Niida and Green [37] have shown that half of the 25% amphibole present in a pyrolite at 10–15 kbar decompose through a continuous reaction before the pressure stability of amphibole is reached at 28–30 kbar. Obviously, in a natural mantle, the reactions of Fig. 5 will take place

over a temperature–pressure interval. Over a certain temperature–pressure range reactants and products will both be stable and a broad rather than a sharp dehydration signal will result from each particular reaction.

Although phase A has no direct bearing on the formation of arc volcanism, the position of invariant point 4 (Fig. 5) is essential for transporting H₂O to great depth. When a portion of hydrated peridotitic slab passes a depth of 180 km at temperatures below ca. 600°C, phase A forms directly from serpentine and the contained water will not directly recycle into the mantle wedge.

6. The fate of water released from the subducting lithosphere

Only a portion of the H₂O initially contained in the subducting lithosphere will escape from the slab in the depth range suitable for arc magma formation. A large portion of H₂O will be dehydrated at relatively shallow levels and a small portion will fade into the deeper mantle. In the following we calculate estimates for the different final destinies of subducted water.

6.1. Oceanic crust

Blueschists of basaltic origin representing shallow portions of subduction zones (10–20 km) have typically 5–6 wt% H₂O bound in hydrous phases. With a 7 km thick mafic oceanic crust, composed by equal parts of basalt and gabbro, 0.5–0.6 × 10⁹ g H₂O m⁻² are bound in the basaltic layer² at shallow depth. Oceanic gabbros are only partially hydrated; with 20–30% hydration by volume we estimate 0.11–0.18 × 10⁹ g H₂O m⁻² for the gabbroic layer. An additional amount of 0.01–0.02 × 10⁹ g H₂O m⁻² will be subducted in the sedimentary layer (200–400 m thick). Some trace elements characteristics for arc volcanism originate mostly from this sedimentary layer; however, its contribution to the H₂O budget is largely within the error of the estimates for the other layers of the oceanic lithosphere.

² In the calculations we use a vertical section through the subducting crust with a unit area of 1 m², thus this number represents the quantity of water in a column of 1 m².

In a vertical section of 1 m², typical dehydration rates between 20 and 70 km depth amount to 0.8 ± 0.2 × 10⁷ g H₂O per kilometre of depth. When the oceanic crust reaches depths of 70–80 km the resulting lawsonite-eclogites (cold subduction zones) or zoisite-eclogites (relatively warm subduction zones, ‘warm’ being intended as just below the wet solidus of the oceanic crust) retain 1 or 0.5 wt% H₂O, i.e. 0.2 or 0.1 × 10⁹ g H₂O m⁻², respectively. If lawsonite-eclogites persist to the maximum depth of lawsonite stability (cold subduction zones), 0.02–0.08 × 10⁹ g H₂O m⁻² will descend to 260–280 km depth and may be lost for arc volcanism (Figs. 7 and 8). At ca. 200 km depth, typical dehydration rates in the stability field of lawsonite are in the order of 0.05–0.09 × 10⁷ g H₂O per km depth, i.e. one order of magnitude lower than at shallow levels.

6.2. Mantle wedge peridotite overlying the oceanic crust

Here, the only hydrous phase which may persist below the depth of arc volcanism is chlorite (Fig. 7). Thermal models indicate that at depth below the volcanic arc a narrow zone of 1–3 km may contain chlorite in cold subduction zones yielding a quantity of 0.06 to 0.16 × 10⁹ g H₂O m⁻². The rest (60–90%) of the previously dehydrated 0.4 to 0.6 × 10⁹ g H₂O m⁻² from the oceanic crust remains mostly in the cold corner of the mantle wedge and a portion of this H₂O will give rise to serpentine diapirs.

6.3. Subducting peridotite underlying the oceanic crust

With a maximum amphibole content of 19 wt% in lherzolite the amount of H₂O bound in amphibole may not exceed 0.5 wt% of the bulk rock. To achieve a similar bulk H₂O content due to serpentinization, only 3 wt% serpentine are necessary. A serpentinization of 3% causes the density of a lherzolite to decrease from 3.30 to 3.28 g/cm³, a negligible effect. Even 10% serpentinization (resulting in 1.3 wt% H₂O in the bulk rock) cause only a small decrease in density from 3.30 to 3.23 g/cm³. Direct information on the extent of serpentinization below the oceanic crust is not available. Serpentine certainly forms at transform faults and fracture zones

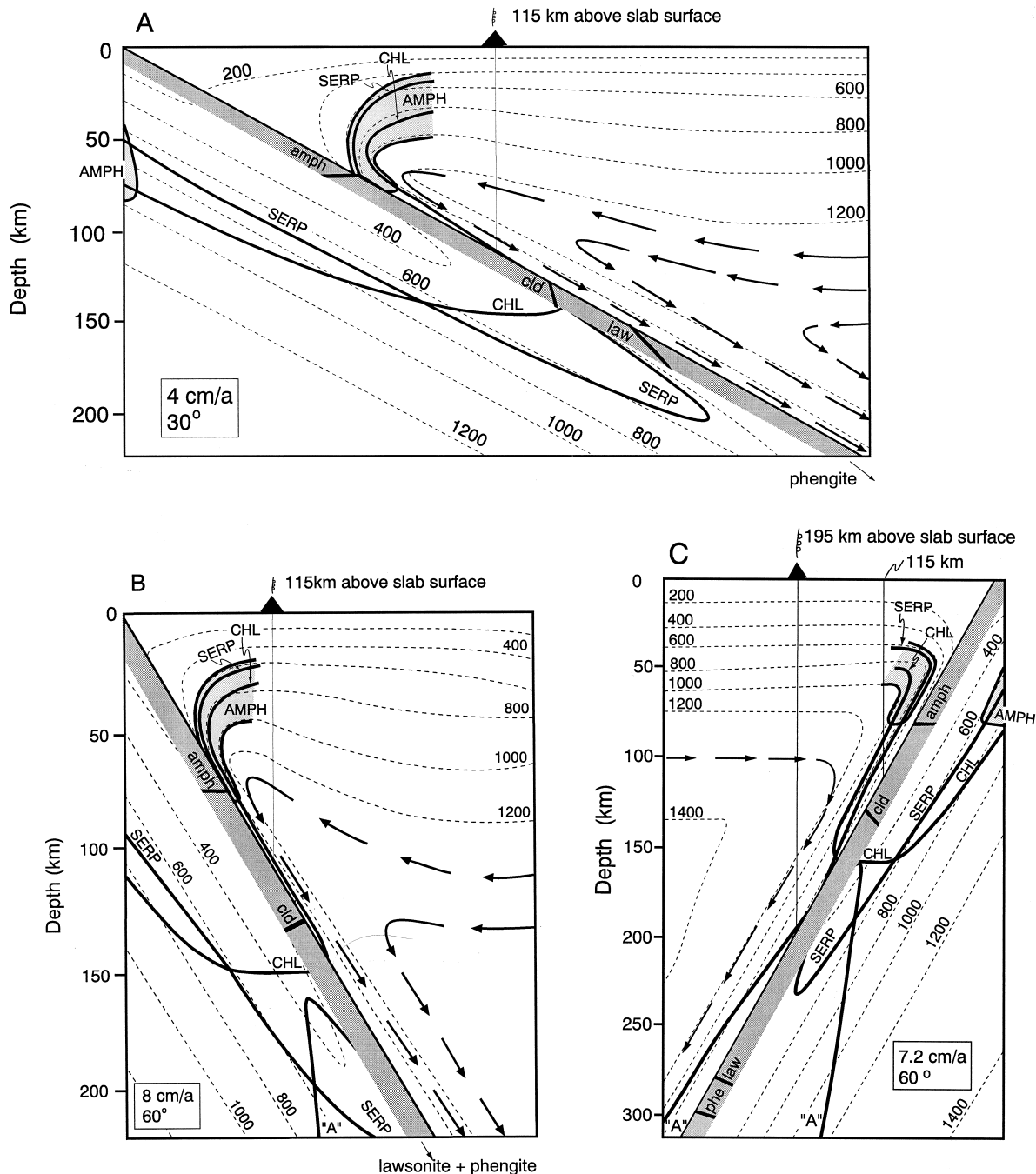


Fig. 7. Stability of hydrous phases for thermal structures with subduction parameters spanning most of the range of modern circum-Pacific subduction zones. Amphibole in peridotite is stable within the light-grey-shaded area (note that at temperatures below 450–500°C diopside is stable instead of tremolitic amphibole). Thermal model of [22] (A and B), and of [47] (C). Stippled lines are isotherms and bold arrows indicate flow lines in the mantle wedge. The principal difference between these two models is the much lower corner flow in (C) [47] which leads to a significantly colder peridotite overlying the oceanic crust. The stability limits of hydrous phases in the subducting peridotite underlying the oceanic crust do not imply that these hydrous phases are present deep into the subducting peridotite. Abbreviations as in Figs. 1 and 5; labels in capital letters mark stability boundaries in peridotite.

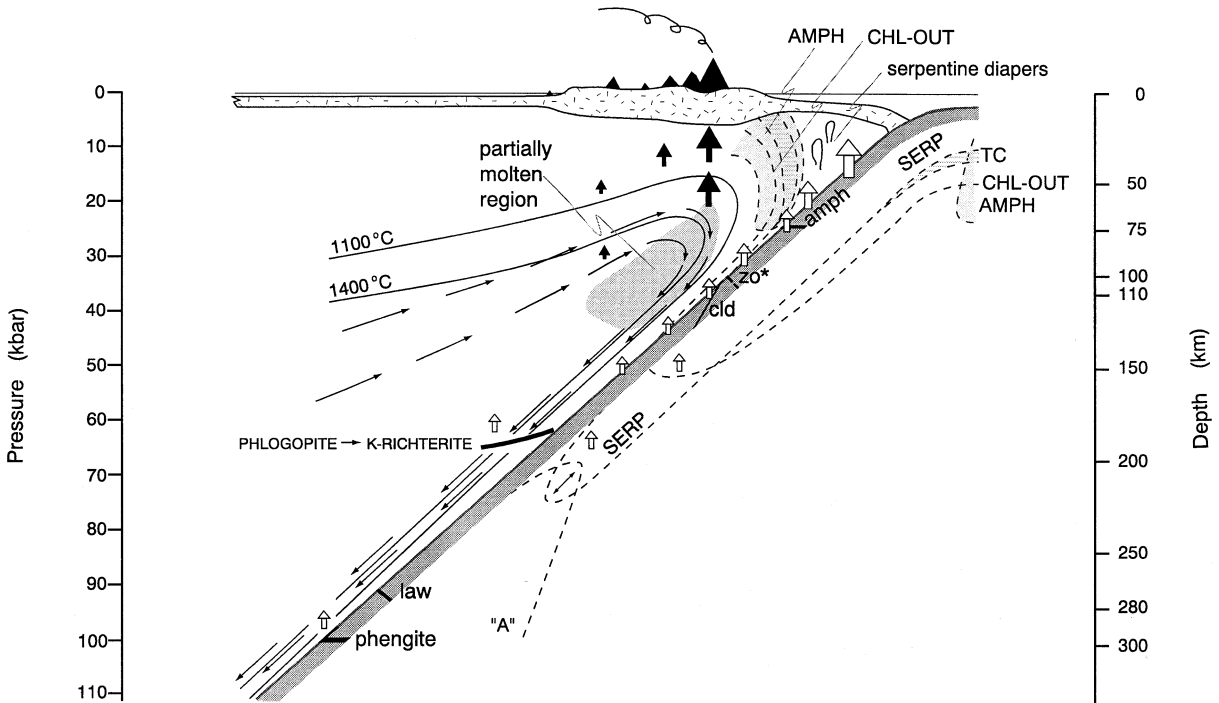


Fig. 8. Model for the formation of the volcanic front. Dehydration from peridotite and oceanic crust occurs at almost any depth to ca. 150–200 km, thus water will be generally available above the subducting lithosphere. The grey region in the mantle wedge will have a significant amount of melt present. The volcanic front forms where the amount of melt is sufficient to mechanically extract and give rise to arc magmatism. Open arrows indicate rise of fluid, short solid arrows indicate rise of melts. Long arrows indicate flow in the mantle wedge. Stippled lines outline stability fields of hydrous phases in peridotite; however, we do not want to imply that peridotite underlying the oceanic crust is fully hydrated. The striped region shows the zone where talc occurs in average peridotite compositions. In some thermal structures (Fig. 7b and c) a portion of the peridotitic lithosphere will be colder than 600°C at 62 kbar, serpentine will react to phase A and thus H₂O will be subducted to large depth. In the oceanic crust, temperatures can be low enough to preserve lawsonite and phengite to their maximum pressure stability; however, at somewhat warmer conditions (slower subduction, shallower angle, younger crust) zoisite (zo*) will be the last potassium-free phase to decompose and the top of the oceanic crust (phengite rich sedimentary layer) might melt. Single phase transitions which cause a potassium-rich fluid pulse could be constituted by the pressure breakdown of phengite in oceanic crust and by the phlogopite to K-richertite reaction in previously K-metasomatized mantle.

which subduct together with undisturbed ocean floor. It was estimated that about 20% of the Pacific Ocean floor are effected by fracture zones [39] and alteration and serpentinization was found to be extensive in ocean basins [40]. We assume a shallow zone of ca. 5 km depth with an average serpentinization of 10% which amounts to $0.21 \times 10^9 \text{ g H}_2\text{O m}^{-2}$. As an upper limit, this value might be doubled, but then the serpentinized peridotite becomes increasingly buoyant ($\rho = 3.15 \text{ g/cm}^3$ for 20% serpentinization) and it becomes questionable if such a peridotite might still be able to descend. Less than half of the above value appears to be inconsistent with the degree of serpentinization observed at modern seafloors. Obviously,

the hydrated peridotite below the oceanic crust cannot be water-saturated (full serpentinization). Thus, in cold subduction zones where the stability fields of phase A and serpentine overlap, H₂O would entirely descend to a large depth and will not be available for arc magmatism. It is only in intermediate to warm subduction zones where fluid will result from serpentine dehydration (Fig. 7). Temperatures in the peridotite of the subducting oceanic lithosphere are lower than in the subducting crust, thus, significant dehydration of this portion of the subducting lithosphere does not take place at shallow levels. At depths where the oceanic crust contains 0.5–2.0 wt % H₂O, the underlying peridotite might well be a reser-

voir of water with a mass of H_2O similar or superior to the H_2O bound in oceanic crust.

6.4. The H_2O -budget

The above calculations show that the oceanic lithosphere contains about $0.71\text{--}1.08 \times 10^9 \text{ g H}_2\text{O m}^{-2}$ at 20 km depth. Both the hydration state of the unmetamorphosed oceanic crust and the early diagenetic processes (e.g. expulsion of pore water [41]) in and below the accretionary prism are extremely difficult to quantify. Thus, we prefer to define the ‘input’ into subduction zones through the state of the oceanic lithosphere at 20 km depth. Our estimate is higher than the $0.3 \times 10^9 \text{ g H}_2\text{O m}^{-2}$ of Peacock [42] which did not consider serpentinization below the oceanic crust and based his estimate on the few DSDP drill holes which perforated into the crystalline oceanic crust. It was pointed out by Bebout [41] that this latter procedure may significantly underestimate the volatile content of subducted crust.

The summation of the above estimates yield the following picture for the amount of H_2O available for arc volcanism. In cold subduction zones, 0.12 to $0.18 \times 10^9 \text{ g H}_2\text{O m}^{-2}$ will rise from the oceanic crust and 0.06 to $0.16 \times 10^9 \text{ g H}_2\text{O m}^{-2}$ will rise from the peridotitic layer above the oceanic crust. Thus, the total amounts to 0.18 to $0.34 \times 10^9 \text{ g H}_2\text{O m}^{-2}$ since no dehydration occurs below the oceanic crust. In intermediate to warm subduction zones, about $0.1 \times 10^9 \text{ g H}_2\text{O m}^{-2}$ will rise from the oceanic crust and roughly 0.1 to $0.3 \times 10^9 \text{ g H}_2\text{O m}^{-2}$ from the peridotite below the oceanic crust. Thus, the total amounts to 0.2 to $0.4 \times 10^9 \text{ g H}_2\text{O m}^{-2}$ since no dehydration occurs above the oceanic crust. It follows that between 18 and 37% of the 0.7 to $1.1 \times 10^9 \text{ g H}_2\text{O m}^{-2}$ present at 10–20 km depth are available for the generation of arc magmas. This portion of H_2O will rise into the mantle wedge in the depth interval between 80 and 150 km. An interesting feature of the above estimate is that there is no principal difference for the recycling rate of water in the volcanic arc between a cold and a warm subduction zone (‘warm’ always being intended as temperatures of the oceanic crust just below its solidus). The above result is higher than estimates that globally 10% to 20% of the subducted water is expelled via arc magmatism [42,43]. However, not all of the water dehydrated

below the arc region will appear at the surface, one portion of the dehydrated water will remain in the mantle wedge.

The above estimates also yield that 30–70% or 0.25 to $0.7 \times 10^9 \text{ g H}_2\text{O m}^{-2}$ of the initially subducted H_2O will be released to the cold corner of the mantle wedge where serpentine is stable. According to the thermal models of Furukawa [22] this region has cross-sections of ca. $3.1 \times 10^9 \text{ m}^2$ for a 30° subduction angle and of 0.7 to $0.9 \times 10^9 \text{ m}^2$ for a 60° subduction angle ($4\text{--}8 \text{ cm/a}$ subduction rates). Full serpentinization (and chloritization) of the cold corner requires about $0.2 \times 10^6 \text{ g H}_2\text{O m}^{-3}$, the bulk rock density would be 2.88 g/cm^3 . For a stationary cold corner, full serpentinization (and chloritization) would be achieved after subduction of $570\text{--}790 \text{ km}$ slab for a 30° subduction angle and $130\text{--}220 \text{ km}$ slab for a 60° subduction angle.

7. Consequences of the experimentally based water budget for the formation of the volcanic front

In the following we discuss models for the formation of volcanic fronts in the light of our water budget. We focus exclusively on arcs where parent magmas form from melting of the mantle wedge and do not discuss slab-derived melts. Such direct melting of the oceanic crust (for models see Ref. [44]) and subsequent adakitic magmatism may only occur when very hot young crust is subducted and is rare on the modern Earth [45].

7.1. ‘Single phase dehydration models’ and the role of amphibole for arc magmatism

Many models for the formation of arc magmatism have been proposed in the last two decades. Some of these models involve a multistage process which evokes dehydration of the slab at a relatively shallow depth and intermediate storage of H_2O (and trace elements deriving from the subducted slab) in a single, key hydrous phase in the mantle wedge. Subsequently it is either proposed that the down-dragged mantle wedge dehydrates and melting occurs above this dehydration zone or that melting of the mantle wedge occurs on the wet solidus of peridotite.

A number of hydrous phases have been called on to explain such transient storage of H₂O and of other ‘metasomatizing components’ within the mantle wedge [30,46,47].

Tatsumi [2,46] and Davies and Stevenson [47] ascribe the distribution maximum of volcanic fronts to the amphibole breakdown in peridotite. Tatsumi assigned the formation of volcanic front to melting within a hydrous column forming directly above amphibole dehydration in peridotite at ca. 110 km depth. Davies and Stevenson [47] evoked a mechanism of lateral transport of water in the mantle wedge. They propose that amphibole dehydrates at ca. 90 km depth but the rising fluid (or melts) rehydrates the convecting mantle wedge and again forms amphibole. Through such a stepwise process water was thought to be transported laterally within the hot wedge. Both these amphibole-based models are in disagreement with available experimental and geochemical constraints.

(1) As previously discussed, the breakdown of calcic amphibole in peridotite occurs, as a function of peridotite composition, between 22 and 30 kbar, i.e. between 65 and 90 km depth. A lateral transport mechanism [47] is only possible for a limited horizontal distance because amphibole melts between the 1000 and 1100°C isotherm in the mantle wedge [48] to form high Mg-andesites. Although such magma compositions occur in arcs, they are not candidates for primitive arc magmas. The most primitive magmas in arcs are basalts to picritic basalts. For their generation, temperatures of 1300–1350°C are necessary ([49–51], fig. 5.6 in [46] and references therein). Thus, even though this mechanism is possible, amphibole falls short in transporting laterally water into the source region of basaltic magmas (Fig. 7).

(2) Even when stable, amphibole contributes moderately to the water budget. It follows from the mass balance calculations that amphibole has a relatively small contribution to the water budget of peridotite (0.2–0.5 wt% H₂O of the bulk rock) with respect to the other hydrous phases. Furthermore it decomposes through continuous reactions [37] and its final breakdown depth is extremely sensible to bulk composition.

(3) Gill and Williams [52] described that about 60% of island arc magmas have U–Th disequilibrium due to U-excess. This U-excess is believed

to result from dehydration of the oceanic crust, the preservation of U–Th disequilibrium thus constrains dehydration of the slab to take place less than 350,000 years before eruption of arc magmas. For different arcs, the time interval between U-addition to the magma and eruption was determined to be less than 20,000 to 200,000 years ([4,53] and references therein). The additional time required for ‘lateral transport’ [47] or ‘simple downdrag’ [46] of H₂O through amphibole can be calculated from subduction geometries and velocity fields in the wedge. At high subduction rates of 10 cm/a and maintaining this high velocity between subducted crust and melting region in the mantle wedge, 460,000 years (60° angle of subduction) to 700,000 years (30° angle of subduction) are necessary for H₂O transport through amphibole to a position below the volcanic front. Because the convection velocity in the mantle wedge is much slower than the velocity of the subducted lithosphere, realistic time spans for such transport mechanisms would be 1.5 to 3 times longer (velocity fields from [22,47]) and thus would largely exceed 350,000 years.

We conclude that the role of amphibole is not outstanding with respect to other hydrous phases. Amphibole cannot constitute ‘the’ fluid source situated below the volcanic front.

7.2. Towards a ‘continuous dehydration model’

The phase petrological data indicate that some fluid rises from the subducting slab and hydrates a portion of the overlying mantle wedge at almost any depth to ca. 150–200 km. Phase relationships in mafic and ultramafic lithologies reveal that, at a given depth, several hydrous phases will decompose through either discontinuous or continuous reactions. Since temperature gradients are high (up to 50°C/km) close to the slab surface, most dehydration reactions will be smeared out over a significant depth interval instead of taking place at a distinct depth. Further broadening of the dehydration signal results from (1) local/vertical inhomogeneities in bulk composition cause different solid phase compositions and consequently dehydration reactions take place at slightly varying *P*–*T* conditions, and (2) uneven H₂O distribution in coronitic metagabbros and metaperidotites. As a consequence, sections through

natural subducting lithosphere will have an even more continuous dehydration signal than indicated by our investigated basalt–H₂O and peridotite–H₂O systems. It should be noted that, independent from phase equilibria data, several recent geochemical studies on modern arcs [6,54,55] equally propose a continuous dehydration of the subducting lithosphere on the basis of trace element and isotopic data.

Dehydration at low pressures is almost entirely due to potassium-free phases, whereas at pressures above 30 kbar, phengite becomes more and more important. The extensive pressure stability of phengite [9,26] indicates that it is more difficult to recycle potassium from the slab than descending potassium to the breakdown depth of phengite (270–300 km). Two continuous processes will allow to recover a portion of the potassium (and related elements). (1) A continuous formation of K-clinopyroxene from phengite liberates water (and thus hydrophile elements such as potassium). This reaction becomes efficient only above 50 kbar. (2) Potassium loss in the oceanic sediments and basalts could be obtained by leaching of hydrophile elements by fluids rising from the lower part of the oceanic crust or the hydrated subducting peridotite through the sedimentary layer.

Consequently H₂O-rich fluids with a variable geochemical signal will be generally available above subducting lithosphere to at least 150–200 km depth (Fig. 8).

The next question to answer is ‘where does the volcanic front form?’ Kushiro [49] suggested that a significant amount of melt forms and collects at the trench-nearside of the partially molten region and deduced that the volcanic front simply forms above the trench-nearest partially molten mantle wedge. Temperatures for attainment of melting in the mantle wedge below volcanic fronts can be deduced from primary arc magmas. Primitive arc magmas from the Earth’s surface and experiments on such magmas (which must be in equilibrium with mantle compositions) indicate mantle wedge temperatures of 1300–1350°C [46,49–51]. Although the quantity of primitive magmas in arcs is small, the very existence of these magmas shows that such temperatures exist below the volcanic arc. Thus, most likely the temperature necessary for mechanical extraction of parental arc magmas is achieved at 1300–1350°C. Therefore the location of the volcanic front is expected to de-

pend mostly on the position of the 1300°C isotherm and (Fig. 8) on the individual subduction parameters which determine the mantle wedge structure.

Unfortunately only few models deal in detail with the concurrent solution of both thermal and mechanical properties of the mantle wedge. The geometry of velocity fields in the wedge and therefore the evolution of the thermal structure close to the ‘magic corner’ mostly depend on the degree of coupling between the subducting slab and the wedge, on mantle wedge viscosity, and on the thickness of the rigid mechanical lithosphere (compare models in [22,47] and [56]). The attainment of mantle wedge temperatures of 1300°C below volcanic arcs are obtained when a vigorous, convective return flow is enhanced either by decoupling and/or progressive thinning of the mechanical lithosphere. A number of other parameters such as convergence rate, dip angle of the slab, age of the slab and initial temperature profile obviously play a major role in determining the magnitude of such return flow [56]. Without a significant corner flow below volcanic fronts mantle wedge temperatures would rapidly cool down and arc magmatism would cease. Seismic tomography and heat flow distribution in Japan are among the most striking evidences which support that such induced flow drives hotter isotherms into the corner ([22,56] and references therein).

Thus, a model where the location of melting in the mantle wedge determines the position of the volcanic front [49] would be consistent with natural observations.

Acknowledgements

We would like to thank O. Sigmarsson and P. Ulmer for discussions. The first version of the manuscript was prepared as M.W. Schmidt was a guest at Tokyo Institute of Technology. Many thanks for enlightening discussions with S. Maruyama. [*CLJ*] [*FA*]

References

- [1] J. Gill, *Orogenic Andesites and Plate Tectonics*, Springer, New York, 1980, 390 pp.

- [2] Y. Tatsumi, Formation of the volcanic front in subduction zones, *Geophys. Res. Lett.* 17 (1986) 717–720.
- [3] J.D. Morris, W.P. Leemann, F. Tera, The subducted component in island arc lavas: constraints from Be isotopes and B–Be systematics, *Nature* 344 (1990) 31–36.
- [4] O. Sigmarsson, M. Condomines, J.D. Morris, R.S. Harmon, Uranium and ^{10}Be enrichments by fluids in the Andean arc magmas, *Nature* 346 (1990) 163–165.
- [5] T. Plank, C.H. Langmuir, Tracing trace elements from sediment input to volcanic output at subduction zones, *Nature* 362 (1993) 739–743.
- [6] T. Ishikawa, E. Nakamura, Origin of the slab component in arc lavas from across-arc variation of B and Pb isotopes, *Nature* 370 (1994) 205–208.
- [7] A.V. Sobolev, M. Chaussidon, H_2O concentrations in primary melts from supra-subduction zones and mid-ocean ridges: implications for H_2O storage and recycling in the mantle, *Earth Planet. Sci. Lett.* 137 (1996) 45–55.
- [8] S. Poli, The amphibolite–eclogite transformation: an experimental study on basalt, *Am. J. Sci.* 293 (1993) 1061–1107.
- [9] M.W. Schmidt, Experimental constraints on recycling of potassium from subducted oceanic crust, *Science* 272 (1996) 1927–1930.
- [10] S. Poli, M.W. Schmidt, H_2O transport and release in subduction zones: experimental constraints on basaltic and andesitic systems, *J. Geophys. Res.* 100 (1995) 22299–22314.
- [11] D.C. Rubie, S. Karato, H. Yan, H.St.C. O'Neill, Low differential stress and controlled chemical environment in multi-anvil high pressure devices, *Phys. Chem. Miner.* 20 (1993) 315–322.
- [12] M.J. Apted, J.G. Liou, Phase relations among greenschist, epidote–amphibolite, and amphibolite in a basaltic system, *Am. J. Sci. A* 283 (1983) 328–354.
- [13] A.R. Pawley, J.R. Holloway, Water sources for subduction zone volcanism: new experimental constraints, *Science* 260 (1993) 664–667.
- [14] B. Messiga, M. Scambelluri, Retrograde P–T–t path for the Voltri Massif eclogites (Ligurian Alps, Italy): some tectonic implications, *J. Metamorph. Geol.* 9 (1991) 93–109.
- [15] A.I. Okay, Mineralogy, petrology, and phase relations of glaucophane-lawsonite zone blueschists in the Tavsan region, Northwest Turkey, *Contrib. Mineral. Petrol.* 72 (1980) 243–255.
- [16] B.C. Storey, A.W. Meneilly, Petrogenesis of metamorphic rocks with a subduction–accretion terrane, Signy Island, South Orkney Islands, *J. Metamorph. Geol.* 3 (1985) 21–42.
- [17] S.P. Thursten, Structure, petrology, and metamorphic history of the Nome group blueschist terrane, Salmon Lake area, Seward Peninsula, Alaska, *Geol. Soc. Am. Bull.* 96 (1985) 600–617.
- [18] S.W. Faryad, Phase petrology and P–T–t conditions of mafic blueschists from the Meliata unit, West Carpathians, Slovakia, *J. Metamorph. Geol.* 13 (1995) 701–714.
- [19] R.Y. Zhang, J.G. Liou, B.L. Coney, Talc-, magnesite-, and Ti-clinohumite-bearing ultrahigh-pressure meta-mafic and ultramafic complex in the Dabie Mountains, China, *J. Petrol.* 36 (1995) 1011–1037.
- [20] S.M. Peacock, The importance of blueschist → eclogite dehydration reactions in subducting oceanic crust, *Geol. Soc. Am. Bull.* 105 (1993) 684–694.
- [21] J.G. Liou, S. Maruyama, M. Cho, Phase equilibria and mineral parageneses of metabasites in low-grade metamorphism, *Mineral. Mag.* 49 (1985) 321–333.
- [22] Y. Furukawa, Magmatic processes under arcs and formation of the volcanic front, *J. Geophys. Res.* 98 (1993) 8309–8319.
- [23] U. Pognante, Petrological constraints on the eclogite- and blueschist-facies metamorphism and P–T–t paths in the Western Alps, *J. Metamorph. Geol.* 9 (1991) 5–17.
- [24] G.T. Nichols, P.J. Wyllie, C.R. Stern, Subduction zone melting of pelagic sediments constrained by melting experiments, *Nature* 371 (1994) 785–788.
- [25] N. Bencolini, S. Poli, M. Valle, High pressure phase relationships in metapelites: an experimental study, *Terra* 8, Abstr. Suppl. 1 (1996) 7.
- [26] K.J. Domanik, J.R. Holloway, The stability and composition of phengitic muscovite and associated phases from 5.5 to 11 GPa: implications for deeply subducted sediments, *Geochim. Cosmochim. Acta* 60 (1996) 4133–4150.
- [27] B.W. Evans, W. Johannes, H. Oterdoom, V. Trommsdorff, Stability of chrysotile and antigorite in the serpentine multisystem, *Schweiz. Mineral. Petrogr. Mitt.* 50 (1976) 481–492.
- [28] P. Ulmer, V. Trommsdorff, Serpentine stability to mantle depths and subduction related magmatism, *Science* 268 (1995) 858–861.
- [29] B.O. Mysen, A.L. Boettcher, Melting of hydrous mantle, I: Phase relations of natural peridotite at high pressures and temperatures with controlled activities of water, carbon dioxide, and hydrogen, *J. Petrol.* 16 (1975) 520–548.
- [30] K. Bose, J. Ganguly, Experimental and theoretical studies of the stabilities of talc, antigorite and phase A at high pressures with application to subduction processes, *Earth Planet. Sci. Lett.* 136 (1995) 109–121.
- [31] D.M. Jenkins, J.V. Chernovsky, Phase equilibria and crystallochemical properties of Mg-chlorite, *Am. Mineral.* 71 (1986) 924–936.
- [32] R.W. Luth, Is phase A relevant to the Earth's mantle?, *Geochim. Cosmochim. Acta* 59 (1995) 679–682.
- [33] A.R. Pawley, High pressure stability of chlorite: a source of H_2O for subduction zone magmatism, *Terra* 8, Abstr. Suppl. 1 (1996) 50.
- [34] T. Fockenberg, New experimental results up to 100 kbar in the system $\text{MgO} \text{-- } \text{Al}_2\text{O}_3 \text{-- } \text{SiO}_2 \text{-- } \text{H}_2\text{O}$ (MASH): preliminary stability fields of chlorite, chloritoid, staurolite, MgMgAl -pumpellyite, and pyrope, *Bochumer Geol. Geotech. Arb.* 44 (1995) 39–44.
- [35] G.L. Millholen, A.J. Irving, P.J. Wyllie, Melting interval of peridotite with 5.7 per cent water to 30 kilobars, *J. Geol.* 82 (1974) 575–587.
- [36] D.H. Green, Experimental melting studies on a model upper

- mantle composition at high pressure under water-saturated and water-undersaturated conditions, *Earth Planet. Sci. Lett.* 19 (1973) 37–53.
- [37] K. Niida, D.H. Green, Stability and chemical composition of pargasitic amphiboles in MORB pyrolite under upper mantle conditions, *Earth Planet. Sci. Lett.* (in press).
- [38] T.J.B. Holland, R. Powell, An enlarged and updated internally consistent thermodynamic dataset with uncertainties and correlations: the system $K_2O-Na_2O-CaO-MgO-MnO-FeO-Fe_2O_3-Al_2O_3-TiO_2-SiO_2-C-H_2-O_2$, *J. Metamorph. Geol.* 8 (1990) 89–124.
- [39] J. Mammerickx, Large scale undersea features on the northeast Pacific, in: E.L. Winterer, D.M. Hussong, R.W. Decker (Eds.), *The Eastern Pacific Ocean and Hawaii, The Geology of North America*, Vol. N, *Geol. Soc. Am.*, 1989, pp. 5–13.
- [40] T. Juteau, M. Cannat, Y. Lagabrielle, Serpentized peridotites in the upper oceanic crust away from transform zones: a comparison of the results of previous DSDP and ODP legs, *Proc. ODP, Sci. Results* 106 (1990) 303–312.
- [41] G.E. Bebout, Volatile transfer and recycling at convergent margins: mass-balance and insights from high-P/T metamorphic rocks (overview), in: G.E. Bebout, D.W. Scholl, S.H. Kirby, J.P. Platt (Eds.), *Subduction, Top to the Bottom*, Am. Geophys. Union, *Geophys. Monogr.* 96.
- [42] S.M. Peacock, Fluid processes in subduction zones, *Science* 248, 329–337.
- [43] E. Ito, H. Harris, A.T. Anderson, Alteration of oceanic crust and geologic cycling of chlorine and water, *Geochim. Cosmochim. Acta* 47 (1983) 1613–1624.
- [44] P.J. Wyllie, Constraints imposed by experimental petrology on possible and impossible magma sources and products, *Philos. Trans. R. Soc. London A* 310 (1984) 439–456.
- [45] H. Martin, Effect of steeper Archean geothermal gradient on geochemistry of subduction-zone magmas, *Geology* 14 (1986) 753–756.
- [46] Y. Tatsumi, S. Eggins, *Subduction Zone Magmatism*, Blackwell, Oxford, 1995, 211 pp.
- [47] J.H. Davies, D.J. Stevenson, Physical model for the source region of subduction zone volatiles, *J. Geophys. Res.* 97 (1992) 2037–2070.
- [48] K. Hirose, Melting experiments on lherzolite KLB-1 under hydrous conditions and generation of high-magnesian andesite melts, *Geology*, Jan. issue 1997.
- [49] I. Kushiro, A petrological model of the mantle wedge and lower crust in the Japanese island arcs, In: B.O. Myrsen (Ed.), *Magmatic Processes: Physicochemical Principles*, *Geochem. Soc. Spec. Publ.* 1 (1987) 165–181.
- [50] P. Ulmer, High-pressure phase equilibria of a calc-alkaline picro-basalt: implications for the genesis of calc-alkaline magmas, *Carnegie Inst. Washington Yearb.* 88 (1988) 28–35.
- [51] E. Takahashi, T. Shimazaki, Y. Tsuzaki, H. Yoshida, Melting study of a peridotite KLB-1 to 6.5 GPa, and the origin of basaltic magmas, *Philos. Trans. R. Soc. London A* 342 (1993) 105–120.
- [52] J.B. Gill, R.W. Williams, Th isotope and U-series studies of subduction-related volcanic rocks, *Geochim. Cosmochim. Acta* 54 (1990) 1427–1442.
- [53] T. Elliot, T. Plank, A. Zindler, Element transport from slab to volcanic front at the Mariana arc, *J. Geophys. Res.* 102 (1997) 14991–15019.
- [54] T. Shibata, E. Nakamura, Across-arc variations of isotope and trace element compositions from Quaternary basaltic volcanic rocks in northeastern Japan: implications for interaction between subducted oceanic slab and mantle wedge, *J. Geophys. Res.* 102 (1997) 8051–8064.
- [55] T. Ishikawa, F. Tera, Distribution and composition of slab derived fluid in the Kurile mantle wedge: constraints from across-arc and along-arc variations of B/Nb and B isotopes, *Earth Planet. Sci. Lett.* (in press).
- [56] C. Kincaid, I.S. Sacks, Thermal and dynamical evolution of the upper mantle in subduction zones, *J. Geophys. Res.* 102 (1997) 12295–12315.
- [57] G.C. Brown, A.E. Mussett, *The Inaccessible Earth, an Integrated View of Its Structure and Composition*, Chapman and Hall, London, 1993.
- [58] A.E. Ringwood, The chemical composition and origin of the Earth, in: P.M. Hurley (Ed.), *Advances in Earth Sciences*, M.I.T. Press, Cambridge, MA, 1966, pp. 287–355.